ELSEVIER

PII: S0032-3861(97)00399-6

Anisotropic behaviour of styrene–butadiene–styrene triblock copolymer/methyl methacrylate–styrene copolymer blends

Ikuro Yamaoka*
New Materials Division, Nippon Steel Corporation, 6-3, Otemachi 2-chome, Chiyoda-ku, Tokyo 100-71, Japan
(Received 20 September 1996; revised 11 April 1997)

Mechanical anisotropy of compression-moulded polymer blends of poly(styrene–*block*–butadiene–*block*–styrene) triblock copolymer (KR05) with methyl methacrylate–styrene copolymer (MS-200) was examined and correlated to microstructure of the blends. The KR05 phase of the blends exhibits lamellar morphology and phase separation from the MS-200 phase. For compression mouldings of the KR05-enriched blends in which most of MS-200 inclusions are relaxed to isotropic spheres the mechanical anisotropy is clearly discernible, consequent on anisotropy of the lamellar arrangement of the KR05 matrix. When KR05 lamellar morphology of the KR05-enriched blends is viewed on scales over the MS-200 domain size, stereoscopic anisotropy of the lamellar orientation is perceived with some disarrayed lamellae in places. Such anisotropy would be prevalent in the mouldings as in compression-moulded KR05, and could occur in somewhat changeable directions of heat transfer on cooling the melt during compression moulding. The mouldings show enhanced toughness when the impact stress is imposed on the mouldings in the direction along which the deformation of the orderly KR05 lamellae may predominate in the whole change of the lamellar morphology on impact. © 1997 Elsevier Science Ltd. All rights reserved.

(Keywords: styrene–butadiene–styrene; lamellar orientation; anisotropy)

INTRODUCTION

Unique characteristics of impact properties and toughening mechanism have been found in commercial polymer blends composed of poly(styrene–*block*–butadiene–*block*–styrene) (SBS) triblock copolymer (KR05, Phillips) with methyl methacrylate–styrene (MS) copolymer (MS-200, Nippon Steel Chemical)[1,2]. Prominent synergistic improvement in impact properties is found when brittle MS-200 domains are incorporated into a ductile KR05 matrix. This can be attained without losing transparency of the two component polymers. The KR05-enriched KR05/MS-200 blend can be referred to as one of 'brittle-in-ductile' type blends[1] which are toughened in a distinct manner from conventional rubber-toughening phenomena[1,2]. When impact stress is imposed on the KR05/MS-200 blends, effective energy dissipation could occur through significant morphological changes in KR05 matrices and around KR05/MS-200 interfaces. Such are the changes that KR05 matrices with alternate lamellar type separation between the polystyrene (PS) and the polybutadiene (PB) phases shear yield with some microstructural cavitation in the PB lamellae, and debond from MS-200 domains in KR05/MS-200 interfacial regions. The synergistic toughening effect is much more striking for compression-moulded KR05/MS-200 blends than for the corresponding injection mouldings due to difference in efficiency of stress dissipation under tension[2]. On impact to the compression-moulded blends,

aligned PB lamellae exhibit dominant rubbery expansion and smooth KR05/MS-200 interfaces debond without excessive stress concentration leading to critical failure. Compared with these, the injection-moulded blends are under two toughening disadvantages, one with corrugated KR05 lamellae where entanglement between PS and PB lamellae disturbs large PB expansion, and the other with undulating KR05/MS-200 interfaces where larger impact stress would be localized and concentrated to limited sites.

The author suggested another singularity of mechanical properties for KR05/MS-200 blends previously[2]. It was found that compression mouldings of KR05-enriched blends show significant mechanical anisotropy while most of the other conventional compression-moulded blends never show that. Indeed drawn films and injection mouldings of conventional polymer blends are very likely to show mechanical anisotropy due to processing-induced orientation of the inclusions[3–5], but once those blends are compression moulded, most of them do not show noticeable mechanical anisotropy[5]. This is because the compression mouldings usually exhibit morphological isotropy of the dispersed domains as a result of very little flow-induced orientation of them during compression moulding. Even if any anisotropic domain morphology is present in the blends before compression moulding, most of the anisotropic domains are more or less relaxed and retracted toward isotropic shape during compression moulding, leading mostly to mouldings without perceivable mechanical anisotropy. Therefore, significant mechanical anisotropy which appears in compression-moulded KR05/MS-200

* Tel.: +81 3 3275 6944; fax: +81 3 3275 6790.

blends is exceptional among conventional compression-moulded blends. If MS-200 domains are dispersed finely in the KR05 matrix, the domains are not primarily responsible for the mechanical anisotropy since most of fine MS-200 domains are well relaxed to isotropic spheres during compression moulding[2]. In this case the mechanical anisotropy should have distinctive correlation with morphological feature of the KR05 matrix. This could be closely related to the lamellar orientation induced by heat transfer on mould cooling, as found for compression-moulded KR05[6].

In this paper, morphological and mechanical anisotropes of compression-moulded KR05/MS2-00 blends have been examined in order to find correlation between the two. Mechanical anisotropy of binary polymer alloys has been examined widely[3-5,7-10], and so has that of block copolymers[6,11-15]. However, it should be noted that mechanical anisotropy of binary polymer alloys containing the block copolymer as one of their constituents has been studied only by few[7].

EXPERIMENTAL

Materials

A commercial star-shaped poly(styrene–*block*–butadiene–*block*–styrene) (SBS) triblock copolymer and a commercial methyl methacrylate–styrene (MS) copolymer used here are the same polymers as chosen in the previous studies[1,2]. The SBS triblock copolymer is manufactured by Phillips under the tradename of K-Resin KR05. The number- and weight-average molecular weights (M_n and M_w), their polydispersity coefficient (M_w/M_n), and the weight fraction (ϕ_w) of a PS block component for KR05 used are 5.23 $\times$ 10^4, 1.51 $\times$ 10^5, 2.89 and 0.755, respectively[1]. KR05 was melt mixed with the MS copolymer supplied by Nippon Steel Chemical under the tradename of MS-200. M_n, M_w, M_w/M_n and ϕ_w of a styrene component for MS-200 used are 1.00 $\times$ 10^5, 2.30 $\times$ 10^5, 2.30 and 0.78, respectively[1]. The polymers were used as received.

Sample preparation

Extrusion. The extruder and extruding conditions were the same that the author adopted previously[1,2]. KR05 was melt mixed with different weight ratios of MS-200 dried in an oven at 80°C for 4 h to avoid hydrolytic degradation. Melt mixing was carried out with a twin screw extruder (partially intermeshing, counter-rotating, $D = 20$ mm and 25D full-flighted screw) at 220°C with a screw speed of 70 RPM Extruded strands were quenched in a water trough and pelletized. As-received KR05 and MS-200 were also extruded to give the same thermal history as for the blends. Pellets extruded once are termed once-extruded pellets as mentioned previously[1,2].

Dried once-extruded pellets were re-extruded in the same way as mentioned above in order to get better dispersion since the extruder used was equipped with no effective mixing sections on full-flighted screws. The degree of mixing of once-extruded KR05/MS-200 blends was improved through re-extrusions[1]. Re-extruded pellets are termed twice-extruded pellets.

The compositions of the blends are indicated as weight percentages KR05/MS-200. For example, KR05/MS-200 (85/15) represents a blend of 85 wt% KR05 and 15 wt% MS-200.

Compression moulding. The pressing machine and moulding conditions were the same that the author

employed before[2]. Twice-extruded pellets were compression moulded at 200°C for 5 min into three types of rectangular plaques of different thickness (150 $\times$ 150 $\times$ 3.0, 4.0 and 6.0 mm), followed by cooling hot moulds. Cooling was carried out by running cold water through pipes in the mould clamping plates of the pressing machine in order for the mould temperature to drop down to 50°C in ca. 3 min. Rectangular plaques 150 $\times$ 150 $\times$ 4.0 mm of once-extruded pellets were compression moulded in the same way, in order to examine the degree of mixing of once-extruded blends.

Right-angled coordinates are put on the moulded plaques as shown in *Figure 1* for stereoscopic analyses. The axes are fixed so that the X direction is identical to the compressive direction and the XZ plane is parallel to the operating side and also the backside of the pressing machine. Plaques moulded of twice-extruded blends were machined into impact (4.0 mm in thickness), tensile (3.0 mm) and flexural (6.0 mm) test bars, respectively. The flexural test bars were also used for deflection temperature measurement under flexural load (DTUL). In order to examine mechanical anisotropy of the compression mouldings, two sets of the test bars were prepared for respective blend compositions and respective mechanical tests employed here. They were cut out of the moulded plaques in the Y and the Z directions, respectively, which meet each other orthogonally. All test bars were cut at inner regions far from the sides of the plaques so that one could ignore the end effect of microdomain structure on mechanical properties. This effect is based on the disturbance of microdomain structure due to melt flow complexity near the mould walls during compression moulding.

Mechanical tests

The notched Izod impact strength of compression mouldings of twice-extruded blends was measured at 23°C according to ASTM D256 using a pendulum type tester. Tensile and three-point loading flexural tests were performed on an Instron testing machine at 23°C according to ASTM D638 and ASTM D790, respectively. The DTUL was measured under a maximum fibre stress of 1820 kPa according to ASTM D648. In order to gauge the mechanical anisotropy, mechanical properties of above-mentioned two sets of test bars were examined.
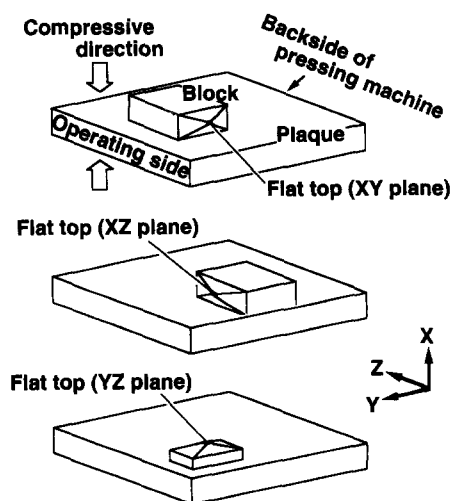
Figure 1 Diagram showing pyramid-shaped pieces cut from compression-moulded plaques. The X axis is fixed in the compressive direction. Flat tops on pieces were made for microtoming parallel to the XY, XZ or YZ plane

Examinations of morphology

Morphology of compression-moulded KR05/MS-200 blends with KR05-enriched composition was observed with transmission electron microscopy. Pyramid-shaped pieces were cut out of inner regions of compression-moulded plaques (4.0 mm thick) as shown in *Figure 1*. Apexes of the pieces were machined from regions close to geometrical centres of the plaques and were cut off to expose surfaces of the plane of interest (*XY*, *XZ* or *YZ* plane) on the resultant flat tops. All the surfaces were made near core regions of the plaques. After treatment with a 2% aqueous solution of osmium tetroxide, ultra-thin sections (500–900 Å in thickness) were microtomed on the flat tops of the pieces using a LKB microtome with a diamond knife. Sections were observed with a Hitachi H700 transmission electron microscope (TEM) at an accelerating voltage of 100 kV, and routine magnifications 30 000× and 100 000× were adopted.

RESULTS AND DISCUSSION

Morphology of compression mouldings of once-extruded blends

In the previous study[2], the morphology viewed on the *XZ* plane of compression-moulded plaques of KR05/MS-200 blends was examined. Here, further examination of morphology of the KR05-enriched blends has been made stereoscopically on the *XY*, *XZ* and *YZ* planes of the plaques in order to know the three-dimensional feature of the morphology. *Figure 2* shows morphology of compression mouldings of once-extruded KR05/MS-200 (85/15) blend. (*a*), (*b*) and (*c*) were taken on the three planes of interest, the *XY*, *XZ* and *YZ* planes, respectively, at core regions of 4.0 mm thick plaques as described in *Figure 1*. Arrows on the micrographs show the *X* direction in which the polymer melt was pressed on compression moulding. As mentioned previously[2], MS-200 domain morphology of compression-moulded KR05/MS-200 blends reflects strongly the degree of mixing for the extruded pellets of which examined plaques were compression moulded. MS-200 domains in compression-moulded plaques of once-extruded KR05/MS-200 (85/15) blend are quite irregular in size and shape, since those in the corresponding once-extruded pellets show wide diversities of size and varied elongations[1]. In the compression mouldings larger and elongated MS-200 domains over 1 μm in size resulted from insufficient mixing of the corresponding once-extruded pellets. MS-200 domains were found irregular-sized and ill-shaped also in compression mouldings of once-extruded KR05/MS-200 (70/30) blend. Compression mouldings of the once-extruded blends with KR05 enriched composition should exhibit such heterogeneous domain morphology.

In addition to a variety of MS-200 domain sizes and shapes, there is another disorder related to the domains, which gives more complexity to MS-200 domain morphology in the blends. The elongated domains in the plaques could vary in the orientation direction, reflecting random arrangement of the pellets with which the plaque mould cavity was charged. The original domain orientation in the pellets is kept roughly in the plaques being compression moulded of the pellets since large shear flow which may change the domain orientation does not occur during compression moulding. Neighbouring MS-200 domains in the moulded plaques would be oriented in much the same direction if seen on a microscopic scale, since in most cases

such domains came from the same pellets. However, orientation directions of the domains distant from one another should look quite various once seen on a macroscopic scale over the size of the pellets with which the mould was charged. The diverse orientation of the elongated MS-200 domains would have a great influence and complicated effects on the mechanical properties and

Figure 2 Transmission electron micrographs of compression mouldings of once-extruded KR05/MS-200 (85/15) blend. The morphology was viewed on sections microtomed on the three different planes which meet at right angles as described in *Figure 1*: (*a*) *XY* plane; (*b*) *XZ* plane; (*c*) *YZ* plane. Pairs of arrows on micrographs show the compressive directions

their anisotropy of compression-moulded plaques of the KR05 enriched blends.

The lamellar orientation itself may be affected by the retracting motion of larger MS-200 domains which intervene among the KR05 matrix, since KR05 should have the lamellar microdomain at the moulding temperature of 200°C[6]. *Figure 2* may not exhibit perceptible morphological anisotropy with respect to KR05 lamellar orderliness, unlike definite lamellar anisotropy seen in compression mouldings of neat KR05[6]. One of the reasons should be ascribed to very long shape relaxation time of large MS-200 domains dispersed in the KR05 matrix. Since MS-200 domains could be phase separated from the KR05 matrix at the temperature on melt processing here (~200°C)[1], shape relaxation of MS-200 domains should be performed in the molten KR05/MS-200 blends during compression moulding. The shape relaxation time is proportionate to the domain size and for the 10 μm-sized MS-200 domains suspended in the KR05 matrix the shape relaxation time at the mould temperature of 200°C is about 12 min, as given in Appendix A. Therefore, the gradual shape retraction of elongated domains of several micrometres or more in size lasted throughout 5-min hot pressing at 200°C and the domain shape could not equilibrate for such a short period. The retraction presumably continued even until the melt temperature fell down to their solidification temperature on subsequent cooling, although the shape relaxation was slowed down due to the increase of the melt viscosity. Such long-lasting motion of very large MS-200 domains could strongly disturb free rearrangement of the surrounding KR05 lamellae present even in the melt state at 200°C during compression moulding[6]. This is probably responsible for the difficulty in discerning whether explicit difference of KR05 lamellar orderliness lies among morphologies viewed on the *XY*, *XZ* and *YZ* planes of the plaque (see *Figure 2*).

Figure 3a–c are higher-magnification views of *Figure 2a–c*, respectively. They were taken at sites apart from very large MS-200 domains more than 10 μm in size, where it is presumed that their shape relaxation during compression moulding did not affect strongly the KR05 lamellar rearrangement. For compression mouldings of once-extruded (85/15) blend, one only just discerns whether difference of KR05 lamellar orderliness lies among morphologies viewed on the *XY*, *XZ* and *YZ* planes of the plaque. It is found to be also the case with compression mouldings of once-extruded (70/30) blend. Accordingly, some degree of stereoscopic anisotropy of the KR05 lamellar arrangement appears in the compression mouldings of once-extruded KR05-enriched blends. KR05 lamellae viewed on the *XZ* and *YZ* planes seem to exhibit a little better orientational regularity in definite directions than those viewed on the *XY* plane, in spite of microscopic disorder of the lamellae just around MS-200 domains[2].

The correlation between domain morphology and mechanical anisotropy of compression mouldings of once-extruded blends is not investigated here because of their morphological complexity as mentioned above in this section.

Morphology of compression mouldings of twice-extruded blends

When neat KR05 was compression moulded into the plaque on the pressing machine used here, significant stereoscopic anisotropy of the microdomain structure was found[6]. KR05 lamellae viewed on the *XZ* and *YZ* planes are

regularly oriented in definite directions whereas those viewed on the *XY* plane are wavy. Here the similar kind of the stereoscopic anisotropy has been found in compression mouldings of twice-extruded KR05-enriched blends.

Figure 4 shows the typical morphology of compression mouldings of twice-extruded KR05/MS-200 (85/15) blend.
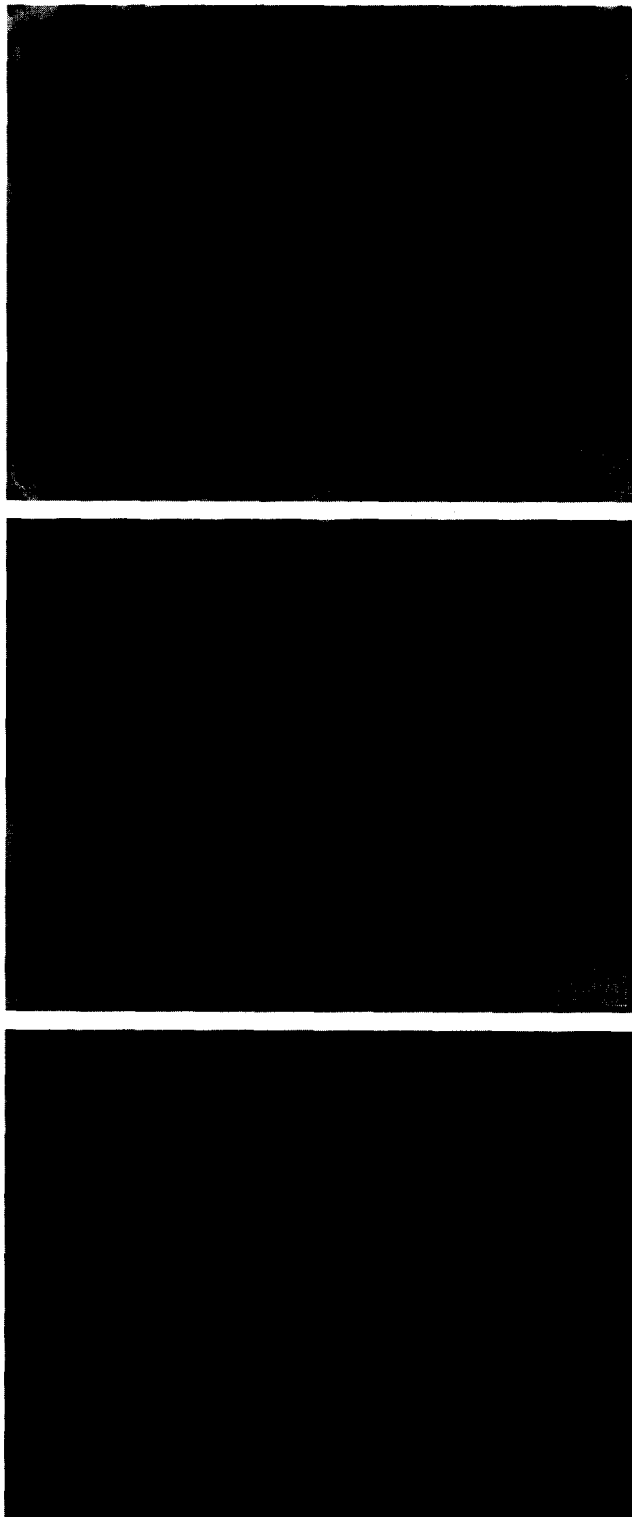
Figure 3 Highly-magnified transmission electron micrographs of compression mouldings of once-extruded KR05/MS-200 (85/15) blend. The morphology was viewed on sections microtomed on the three different planes which meet at right angles as described in *Figure 1*: (a) *XY* plane; (b) *XZ* plane; (c) *YZ* plane. Pairs of arrows on micrographs show the compressive directions. Note that micrographs were taken at sites several to more than ten micrometres away from very large MS-200 domains
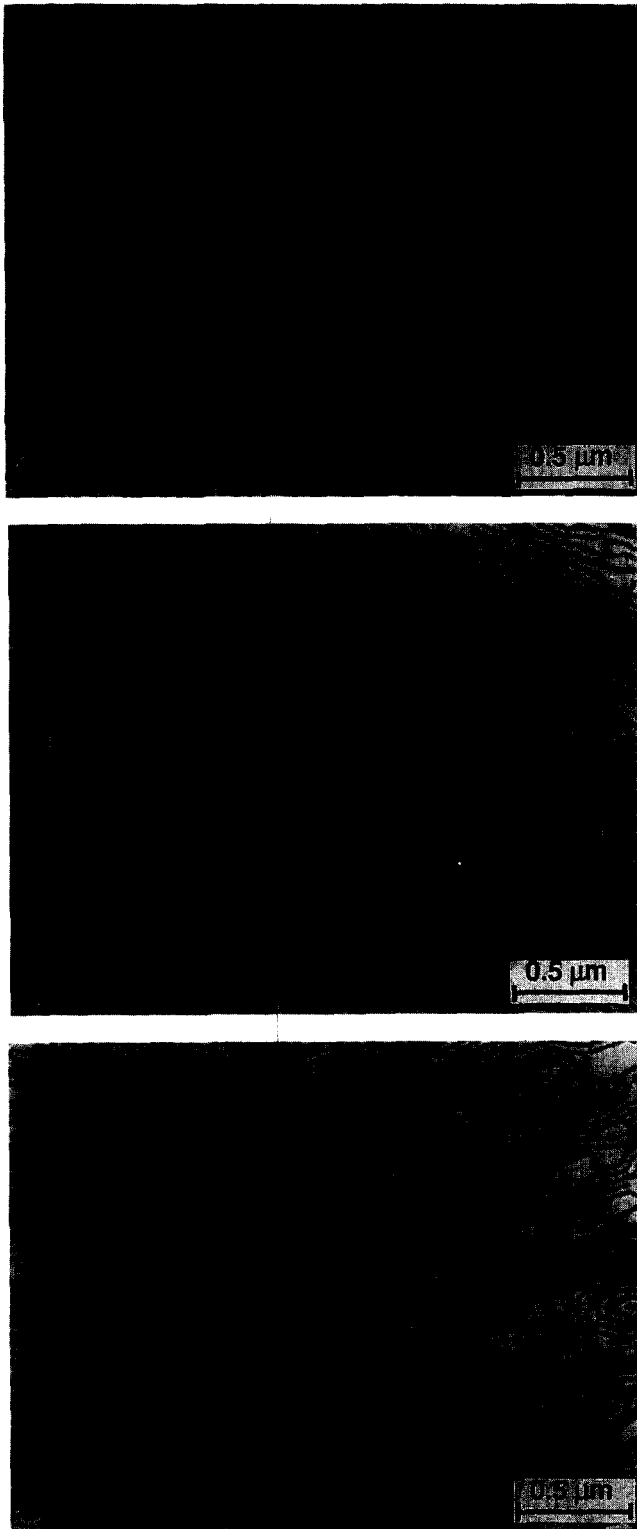
Figure 4 Transmission electron micrographs of compression mouldings of twice-extruded KR05/MS-200 (85/15) blend. The morphology was viewed on sections microtomed on the three different planes which meet at right angles as described in *Figure 1*: (*a*) *XY* plane; (*b*) *XZ* plane; (*c*) *YZ* plane. The compressive directions are shown by pairs of arrows on micrographs

(*a*), (*b*) and (*c*) were taken on the *XY*, *XZ* and *YZ* planes, respectively, at core regions of 4 mm thick plaques as shown in *Figure 1*. Arrows on the micrographs show the *X* direction in which the polymer melt was compressed on moulding. The morphologies are subject to change in places on the *XY*, *XZ* and *YZ* planes, but it should be noted that *Figure 4* shows the morphology well predominant on the

respective planes as examined later in this section. Therefore, overall morphological features could be discussed based on those seen in *Figure 4*. When KR05 lamellar morphology shown in *Figure 4* is viewed on a scale much over the average MS-200 domain size (i.e. a scale over a few micrometres), one can discern clear stereoscopic anisotropy with respect to the orderliness of KR05 lamellae. It has been found that such a feature is also true of compression mouldings of twice-extruded KR05/MS-200 (70/30) blend. Accordingly, the KR05 lamellae viewed on the *XZ* and *YZ* planes of twice-extruded KR05-enriched blends exhibit much better orientational regularity in definite directions than those viewed on the *XY* plane, in spite of inevitable disorder of the lamellar arrangement just around intervenient MS-200 domains[2]. MS-200 domains affected the lamellar orientation only in this way, and did not contribute positively to the formation of the stereoscopic anisotropy because of their isotropic spherical shape. Lamellae on the *XZ* and *YZ* planes appear to be more unidirectional than those on the *XY* plane, leading to definite stereoscopic anisotropy of the microdomain structure. However, when viewed on a scale of the order of the average MS-200 domain size (i.e. a scale of a submicrometre), stereoscopic anisotropy cannot be
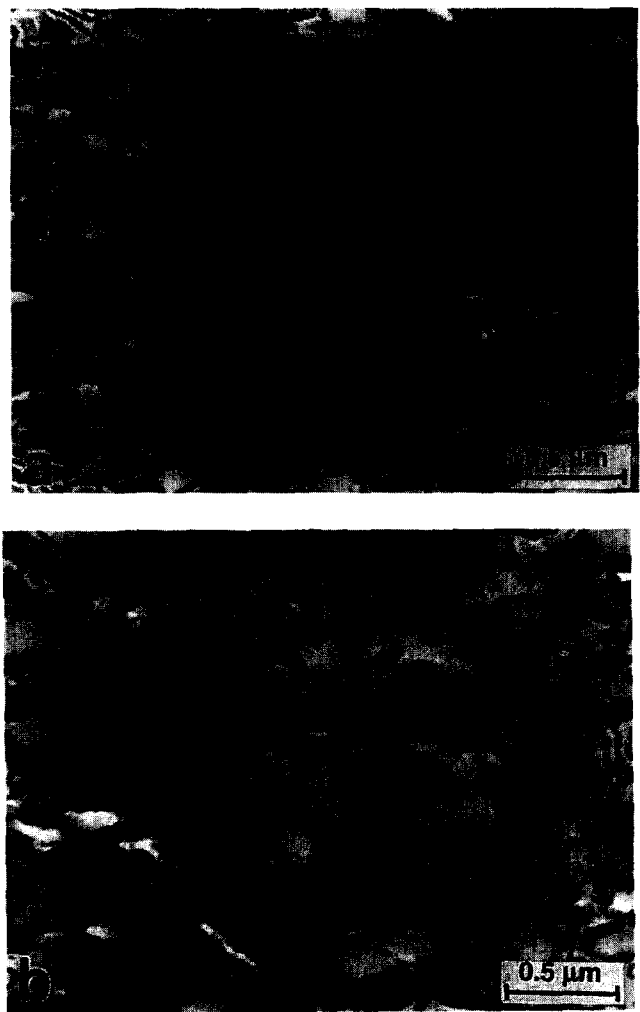
Figure 5 Transmission electron micrographs of compression mouldings of twice-extruded KR05/MS-200 (85/15) blend. Micrographs (*a*) and (*b*) were viewed on sections microtomed on the *XZ* and *YZ* planes tens of micrometres apart from the viewpoints taken for *Figure 4b* and *c*, respectively. The compressive direction is shown by a pair of arrows on (*a*)

distinguished. On this scale KR05 lamellae are not straightforward with intermittent corrugation since the MS-200 domains suspended in the melt could disturb orderly lamellar stratification on cooling the melt[2].

The morphological features significantly different from those as viewed in *Figure 4* were found in places on the *XZ* and *YZ* planes of compression mouldings of the twice-extruded blends. The examples can be shown with *Figure 5a* and *b*, morphologies on the *XZ* and *YZ* planes at the sites tens of micrometres apart from the viewpoints taken for *Figure 4b* and *c*, respectively. Arrows on (*a*) denote the compressive direction (i.e. the *X* direction). In *Figure 4b* and *c* alternate stratification of the stained PB phase and the bright PS phase of the KR05 matrix is seen in the clear stripe pattern, which means that the lamellar normals (the directions perpendicular to the interface between the PB and the PS lamellae) are oriented roughly perpendicular to the sectional normals (the directions perpendicular to the surfaces of the ultra-thin specimens) as far as only the microscopic regions which appear in the figures are examined. However, in *Figure 5* alternate lamellar arrangement of the KR05 matrix is not clearly visible. The KR05 matrix is studded with microscopic parts showing the apparent stripe pattern of the lamellae and many blotchy parts showing no stripe pattern, both of which can be distinguished from intervenient MS-200 domains. Regions with the dark blots must be sectional views microtomed roughly along or obliquely for the orientation direction of the lamellae stained by osmium tetroxide. Such morphological features suggest that the orientation of the lamellar normal fluctuates in planes nearly parallel to the *XY* plane on a microscopic scale. Scanning surfaces of ultrathin sections on the TEM proved that wide expanses of the neat lamellar morphologies are accompanied by the lamellar normals roughly perpendicular to the sectional normals for the surfaces on the *XZ* and *YZ* planes, their morphological features being as viewed in *Figure 4b* and *c*, respectively. However, such widespread morphological uniformities are blurred or intermitted at irregular intervals, presumably at random, by the regional morphologies as exemplified in *Figure 5*. Morphologies with orderly lamellae as viewed in *Figure 4b* and *c* predominate on the *XZ* and *YZ* planes of the compression mouldings of twice-extruded KR05/MS-200 (85/15) blend, respectively. On the *XY* plane of the mouldings, the morphology with undulant lamellae as seen in *Figure 4a* prevails since microscopic regions with ordered lamellae were found only in places when surfaces of ultra-thin sections on that plane were scanned.

The stereoscopic morphology was examined also for compression mouldings of twice-extruded KR05/MS-200 (70/30) blend. When surfaces of ultra-thin sections on the *XY*, *XZ* and *YZ* planes were scanned, the stereoscopic morphology was found to be in the same manner as in the corresponding (85/15) blend. For KR05-enriched blends, accordingly, orderly lamellar morphologies as viewed in *Figure 4b* and *c* could predominate on the *XZ* and *YZ* planes, respectively, while disordered lamellae as viewed in *Figure 4a* could be prevalent on the *XY* plane. It should be noted that local and minor morphology as viewed in *Figure 5* could appear in places on the *XZ* and *YZ* planes.

The discussion here is consistent with the stereoscopic anisotropy of the lamellar orientation found in compression-moulded KR05[6]. *Figure 6a* and *b* show examples of minor morphologies viewed on the *XZ* and *YZ* planes of the compression-moulded plaque of neat KR05, respectively, which are not shown in ref.[6]. Arrows on (*a*) denote the

compressive direction. In *Figure 6* definite stripe patterns of KR05 lamellae are seen only partially, as in *Figure 5*. Scanning sectional surfaces on the *XY*, *XZ* and *YZ* planes of the compression-moulded plaque of KR05 revealed the feature of the stereoscopic anisotropy similar to that of the above-mentioned twice-extruded blends. On the *XZ* and *YZ* planes, the morphologies as shown in *Figure 6* were in the minority and scattered among predominant lamellar morphologies with definite stripe pattern as shown in *Figure 9b* and *c* of ref.[6]. On the contrary disorderly lamellae as shown in *Figure 9a* of ref.[6] were seen prevalently on the *XY* plane.

Several mouldings were examined by transmission electron microscopy to model the stereoscopic morphological structure. Ultra-thin sections were microtomed with care as exactly on the *XY* plane in the *Y* direction as possible so that slight microscratches produced by a diamond knife edge could become references to examine the direction of the lamellar orientation. Similarly the other ultra-thin sections were microtomed exactly on the *XZ* plane in the *X* direction, or on the *YZ* plane in the *Y* direction. The directions of the lamellar orientation relative to the *X*, *Y* or *Z* direction were examined by tracing microscratches seen
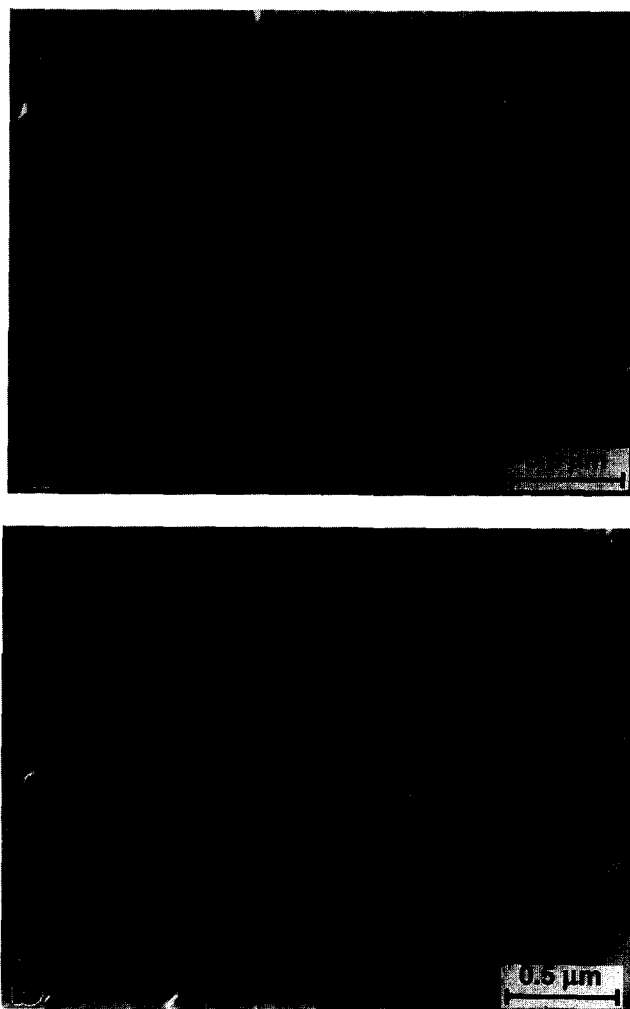
Figure 6 Transmission electron micrographs of compression mouldings of neat KR05 taken on two planes which meet at right angles as described in *Figure 1*: (*a*) *XZ* plane; (*b*) *YZ* plane. These morphologies were found only in places on respective planes while most of morphologies seen on those planes exhibited the orderly and straightforward stratification of the KR05 lamellae as mentioned elsewhere [6]. The compressive direction is shown by a pair of arrows on (*a*)

very slightly on the micrographs in order to model stereoscopic arrangements of KR05 lamellae in the blends. *Figure 7* represents a speculative model showing the stereoscopic morphology of compression-moulded plaques of the KR05-enriched blends. This model reflects spatial morphology of all the test bars well, since they were cut out from the inner regions of moulded plaques where morphological end effects, as mentioned earlier, could be ignored. In this model the KR05 lamellar thickness and the MS-200 domain diameter are exaggerated for plaque size so that the lamellar orderliness can be clearly seen. The lamellae as viewed on the XZ and YZ planes exhibit comparatively regular orientation in spite of intervention of MS-200 domains. They seem to be oriented a little obliquely to the Z direction. However, their orderly stratification is blurred in places by insertions of microscopic regions where the lamellar normals are oriented at random in planes nearly parallel to the XY plane. The majority of the lamellae as viewed on the XY plane are wavier and oriented at random, even at sites away from embedded MS-200 domains. The lamellar morphology seen on the XZ and YZ planes is perceptibly different from that seen on the XY plane, leading to the stereoscopic anisotropy of the lamellar orientation. Such anisotropic structure was more or less reproduced as long as the moulding condition was not changed.

Lamellar rearrangement on compression moulding

It can be presumed that the anisotropic stratification of KR05 lamellae would be performed through the rearrangement of the microdomain orientation at thermal disequilibrium when the polymer melt was cooled in the mould. The mould temperature dropped from 200°C down to 50°C in ca. 3 min as mentioned earlier in this paper. The possible displacement of the molten microdomain of KR05 on cooling the mould ought to be estimated in order to see if this presumption is reasonable. For the first 30 s on cooling, the average diffusion distance L_{ave} of the centre of mass of KR05 molecules in the melt should be over 0.34, 0.40 and 0.48 μm at regions 0.5, 1.0 and 2.0 mm in depth from the surface of a molten 4.0 mm thick plaque, respectively (see Appendix B). Since such distances are comparable to the undulation size of the lamellar disorder, on cooling a greater part of KR05 microdomain structure inside the
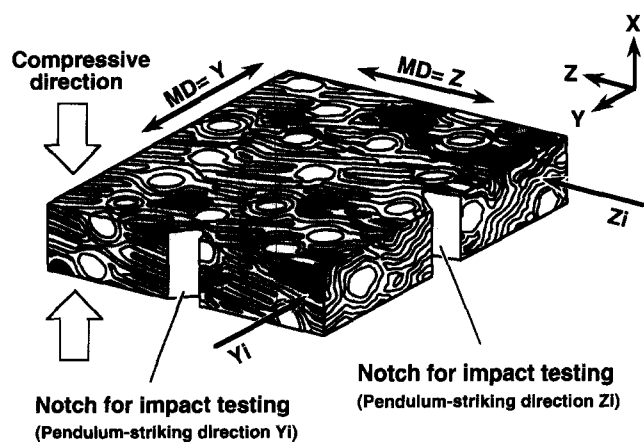
plaque-shaped melt could have the mobility large enough to rearrange the lamellae into the orderly orientation.

The following should be responsible for unbalanced anisotropic stratification of KR05 lamellae appeared in the compression-moulded plaques of the blends. Several researchers observed that when the styrene–diene block copolymers with lamellar or cylindrical phase separations have been cast into films or extruded, their interfaces between the PS and the polydiene phases are oriented roughly parallel to the surfaces of the cast films[16–18] or the extrudates[12,13,19]. These phenomena should be due to gradual one-by-one phase separation or interface rearrangement of the styrene–diene block copolymers which begins at the surface regions of the bulk and proceeds in the thickness direction, since the direction of solvent transfer in the cast films or heat transfer in the extrudates is on the whole perpendicular to their surfaces. From this thermodynamic viewpoint, one can suppose that the similar phenomenon could occur during compression moulding of KR05/MS-200 blends. If heat conducts perpendicular to the plaque surfaces on cooling, PS–PB interfaces of KR05 in the blends may stratify practically perpendicular to the bulk surfaces through the thickness of the mouldings in a pseudo-stationary state. However, in the plaques of the blends studied here, the direction of main heat transfer would not keep perpendicular to the plaque surfaces (i.e. the YZ plane) and vary with time even at the core regions of the plaques. This should result from the unbalanced layout of water-cooling pipes which were embedded in mould clamping plates of the pressing machine used here. No uniform cooling was done with the machine, which is probably the factor most responsible for the partial morphological anisotropy in the compression-moulded plaques of KR05/MS-200 blends, as modeled in *Figure 7*. The KR05 lamellar rearrangement on the XY plane was affected much more than that on the XZ and YZ planes. Undulation of the KR05 lamellae on the XY plane must have occurred in the capriciously swaying direction of heat transfer on cooling the melt.

Figure 7 Speculative model showing stereoscopic microdomain structure of compression-moulded plaques of KR05-enriched KR05/MS-200 blends. Note that the lamellar thickness of KR05 and the domain diameter of MS-200 are greatly exaggerated for plaque dimensions. Arrows Y_i and Z_i exhibit the pendulum-striking directions for impact test bars machined in the Z and Y directions, respectively

Figure 8 Notched Izod impact strength of compression mouldings of twice-extruded KR05/MS-200 blends plotted as a function of MS-200 content. Hollow and solid symbols represent the data for test bars machined in the Y direction and in the Z direction, respectively

Mechanical anisotropy

Figure 8 shows the notched Izod impact strength of compression mouldings of twice-extruded KR05/MS-200 blends. As mentioned previously[1,2], ductile KR05 is toughened by incorporation of brittle MS-200, and synergistic improvement of toughness is observed for the KR05-enriched blends. Another peculiarity related to toughness of the KR05-enriched blends has been found. The test bars machined in the Z direction (solid symbols) are more toughened than those machined in the Y direction (hollow symbols) which meets the Z direction at a right angle. Anisotropy of the impact strength is such that
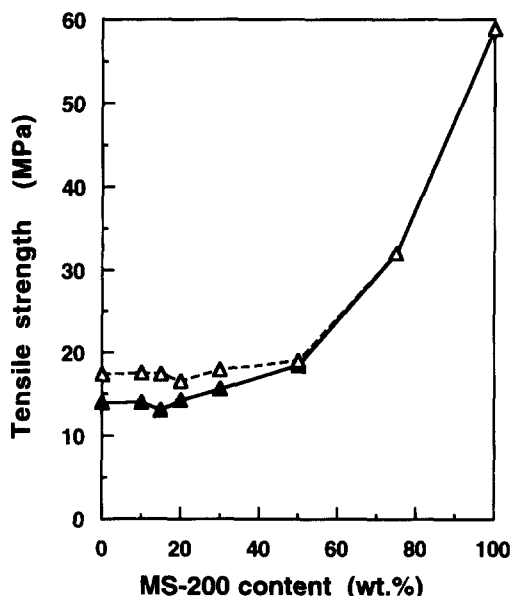
Figure 9 Tensile strength of compression mouldings of twice-extruded KR05/MS-200 blends plotted as a function of MS-200 content. Hollow and solid symbols represent the data for test bars machined in the Y direction and in the Z direction, respectively
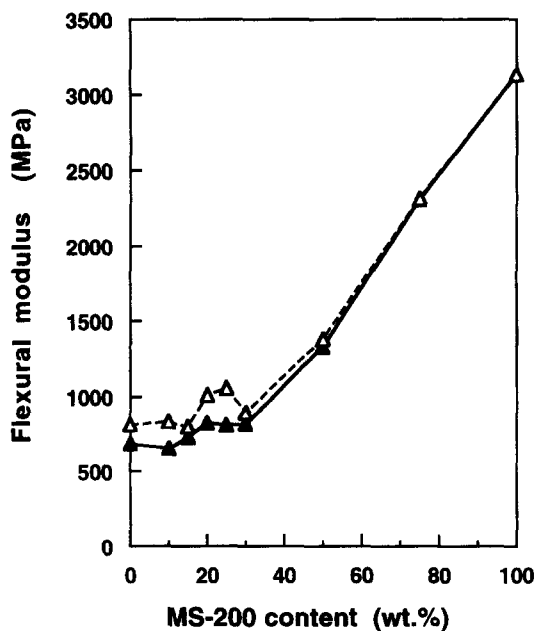
toughness variance depending on the machining direction of the moulded plaques was easily perceived on impact to the KR05-enriched blends. Toughness difference between the bars machined in the Y and the Z directions is enlarged gradually as the KR05 content of the blends increases.

Figure 9 shows the tensile strength of compression mouldings of twice-extruded KR05/MS-200 blends. The flexural modulus and the DTUL of the mouldings are shown in *Figures 10* and *11*, respectively. Symbols used are the same as employed on *Figure 8*. It is shown that the rigidity-related properties of the KR05-enriched blends also vary with the machining direction of the moulded plaques. For the rigidity-related properties superiority lies in the test bars machined in the Y direction (hollow symbols).

The mechanical properties vary depending on the direction in which test bars were machined off. The mechanical anisotropy of compression-moulded KR05/MS-200 blends should be accounted for with the morphological anisotropy, which is discussed below.

Effects of morphology on mechanical anisotropy

Notched Izod impact strength. On Izod impact testing the pendulum-striking direction was normal to the machine direction (MD) of the test bar. Arrows Y_i and Z_i in *Figure 7* exhibit the pendulum-striking directions for impact test bars machined in the Z and Y directions, respectively. *Figures 12* and *13* show the pendulum striking directions and the geometry of impact test bars machined from the compression-moulded plaques of KR05/MS-200 blends in the Z and Y directions, respectively. (*a*) and (*b*) in *Figures 12* and *13* show a front view and a side view of a test bar in a vice of an impact testing machine, respectively. In (*b*), the striking direction is normal to the figure. In *Figures 12* and *13*, images of KR05 lamellar arrangements and MS-200 domains on respective planes are illustrated with the lamellar thickness and the domain size largely exaggerated.

The notched Izod impact strength of the blends is shown

Figure 10 Flexural modulus of compression mouldings of twice-extruded KR05/MS-200 blends plotted as a function of MS-200 content. Hollow and solid symbols represent the data for test bars machined in the Y direction and in the Z direction, respectively
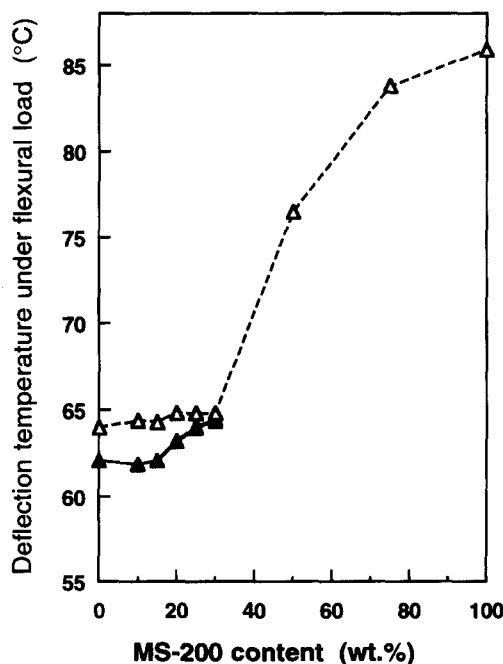
Figure 11 Deflection temperature of compression mouldings of twice-extruded KR05/MS-200 blends under flexural load plotted as a function of MS-200 content. Hollow and solid symbols represent the data for test bars machined in the Y direction and in the Z direction, respectively

(a) Front view   **(b) Side view**
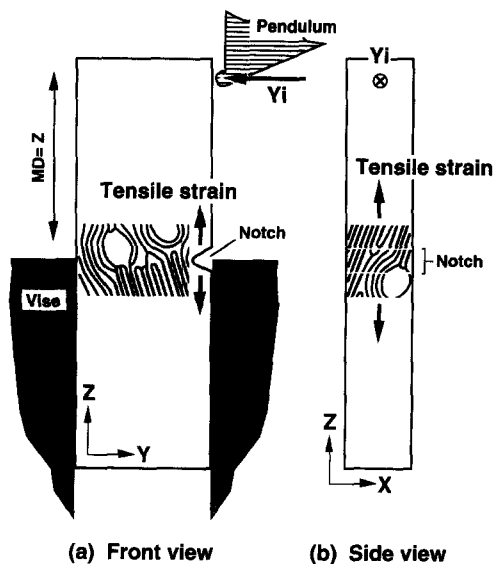
Figure 12 Schematic diagram of pendulum-striking to an Izod impact test bar of KR05-enriched KR05/MS-200 blends machined from a compression-moulded plaque in the Z direction. The striking direction was Y_i. (a) and (b) show a front view and a side view of a test bar in a vice, respectively. In (b), the striking direction Y_i is shown normal to the figure. Images of the microdomain structure on the YZ and XZ planes subjected to tensile strain on impact are illustrated in (a) and (b), respectively. The images exhibit the arrangement of KR05 lamellae among which MS-200 domains intervene. Note that the lamellar thickness of KR05 and the domain diameter of MS-200 are greatly exaggerated for the size of a test bar

(a) Front view   **(b) Side view**
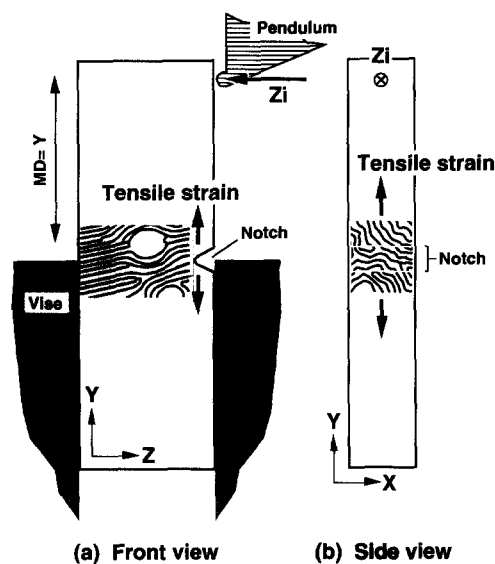
Figure 13 Schematic diagram of pendulum-striking to an Izod impact testbar of KR05-enriched KR05/MS-200 blends machined from a compression-moulded plaque in the Y direction. The striking direction was Z_i. (a) and (b) show a front view and a side view of a test bar in a vice, respectively. In (b), the striking direction Z_i is shown normal to the figure. Images of the microdomain structure on the YZ and XY planes subjected to tensile strain on impact are illustrated in (a) and (b), respectively. The images exhibit the arrangement of KR05 lamellae among which MS-200 domains intervene. Note that the lamellar thickness of KR05 and the domain diameter of MS-200 are greatly exaggerated for the size of a test bar

in *Figure 8*. A set of test bars machined in the Z direction (pendulum-struck in the Y_i direction) showed higher impact strength than another set of bars machined in the Y direction (struck in the Z_i direction). The difference in the deformation process of KR05 lamellae between the two sets could account for the toughness difference. Impact in the Y_i direction gives rise to instantaneous tensile stress in the Z direction at the notch tip zone of the test bar (*Figure 12*). Such stress presumably causes far-reaching microdeforma-

tion in ordered KR05 lamellae on both the XZ and YZ planes. Since the toughening effect is much more striking for the morphology with well-aligned KR05 lamellae than for that with crooked KR05 lamellae[6], a larger amount of impact energy dissipation results. On the other hand, impact in the Z_i direction gives rise to tensile stress in the Y direction at the notch tip zone of the test bar (*Figure 13*). Crooked lamellae viewed on the XY plane could not dissipate dilational impact stress well since the PB phase tangled with the rigid PS phase does not expand largely[6]. Consequently, impact in the Z_i direction would not absorb such large energy as that in the Y_i direction.

Anisotropy of the impact strength is noteworthy for KR05-enriched blends whereas that is hardly seen for the blends with the minor KR05 phase (*Figure 8*). As the MS-200 content of the blends increases, anisotropy of the impact strength becomes less noticeable since neat lamellar arrangement could be disturbed more by larger and more crowded MS-200 domains among the lamellae with increasing the MS-200 content. Partial anisotropy of KR05 lamellar arrangement should have discernible influence on anisotropy of the impact strength at any rate when the KR05 forms a continuous matrix phase, and the influence is great if the MS-200 content is small.

Rigidity-related properties

In the case of tensile testing, the direction of tensile stress application was identical to the MD of test bars as shown in *Figure 14*. In the cases of flexural testing and deflection

(a) MD= Y

(b) MD= Z
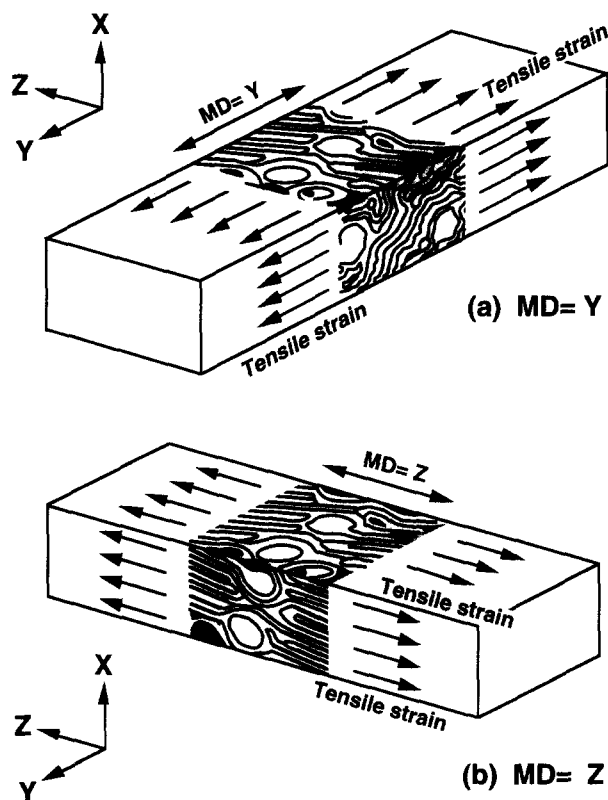
Figure 14 Schematic diagram showing sections of dumbbell-shaped test bars under tension, which were machined from compression-moulded plaques of KR05-enriched KR05/MS-200 blends. (a) and (b) show the bars machined in the Y and the Z directions, respectively. The tensile direction was identical to the machine direction (MD). On the bars, images of the microdomain structure on planes subjected to tensile strain are illustrated. The images exhibit the arrangement of KR05 lamellae among which MS-200 domains intervene. Note that the lamellar thickness of KR05 and the domain diameter of MS-200 are greatly exaggerated for the size of a test bar
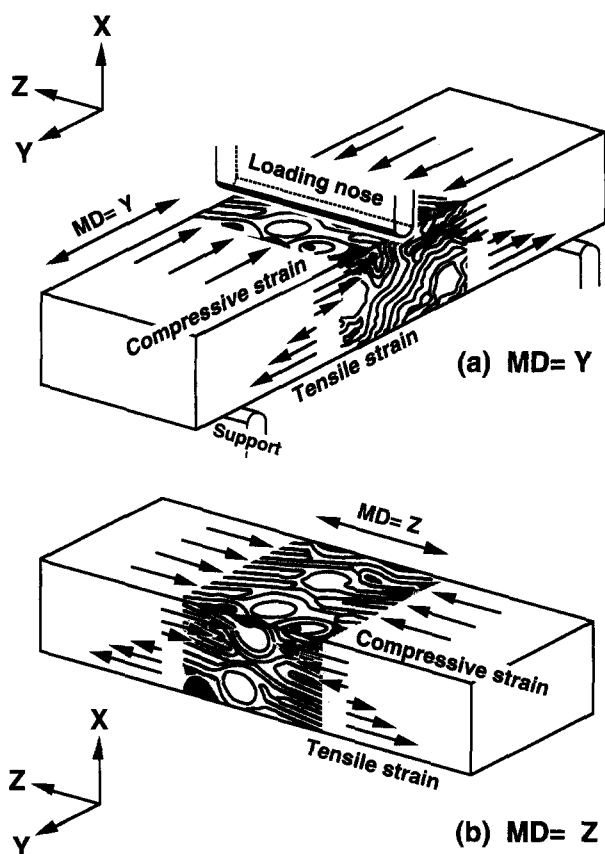
Figure 15 Schematic diagram showing test bars under three-point bending, which were machined from compression-moulded plaques of KR05-enriched KR05/MS-200 blends. (*a*) and (*b*) show the bars machined in the *Y* and the *Z* directions, respectively. The direction of stress application was identical to the machine direction (MD). On the bars, images of the microdomain structure on planes subjected to strain are illustrated. The images exhibit the arrangement of KR05 lamellae among which MS-200 domains intervene. Note that the lamellar thickness of KR05 and the domain diameter of MS-200 are greatly exaggerated for the size of a test bar

temperature measurement, the direction of stress application was also identical to the MD of test bars as shown in *Figure 15*. In these figures, scales of the KR05 lamellar thickness and the MS-200 domain diameter on respective planes are largely exaggerated. It should be noted that on 3-point loading (see *Figure 15*) compressive stress was induced at the upper skin regions in test bars on specimen supports, while tensile stress was induced at the lower skin regions and interlayer shear stress at the core. Test bars machined in the *Y* direction could offer large resistance to plastic deformation since close and complicated networks of the KR05 lamellar matrix are formed on the *XY* plane, which is one of the two planes along which stress was induced extensively on testing. On the other hand, test bars machined in the *Z* direction must have been more easily plastic-deformed because of orderly lamellae viewed on both the *XZ* and *YZ* planes along which stress was induced on testing. These could result in the enhanced strength and modulus of the test bars cut out in the *Y* direction. Their anisotropy could depend on the degree of disturbance of KR05 lamellar orientation by intervenient MS-200 domains, as mentioned for the case of the impact strength of the blends.

CONCLUSIONS

Mechanical anisotropy of compression-moulded KR05/MS-

200 polymer blends was examined and correlated to microstructure of the blends. The KR05 phase of the blends exhibits lamellar morphology and phase separation from the MS-200 phase. For KR05-enriched blends with isotropic spheres of MS-200 inclusions the mechanical anisotropy is definitely discernible, which is due to the stereoscopic anisotropy of the KR05 lamellar arrangement. When KR05 lamellar morphology of KR05-enriched blends is viewed on scales over the MS-200 domain size, the stereoscopic anisotropy can be recognized as seen in compression-moulded KR05. This anisotropy could result from versatile directions of heat transfer on cooling the melt during compression moulding. The mouldings show enhanced toughness when the stress is imposed in the direction along which the deformation of the orderly lamellae may predominate in the whole lamellar deformation. The mouldings show better rigidity-related properties when the stress is imposed in the direction along which the deformation of the disorderly lamellae becomes significant.

APPENDIX A:

For the 10 μm-sized molten MS-200 domain embedded in the molten KR05, the shape relaxation time τ_{shape} is estimated as follows.

For the molten polymer blends composed of inclusions dispersed in the continuous phase, the required time τ_{shape} for inclusions to be relaxed into their equilibrium spherical shape is of the order of $R\eta_m/\gamma_{i-m}$ [20,21], and more exactly [22,23];

$$\tau_{\text{shape}} = (R\eta_m/4\gamma_{i-m})\cdot[(19K + 16)(2K + 3 - 2\phi_v(K - 1))]/$$
$$[10(K + 1) - 2\phi_v(5K + 2)] \qquad (A1)$$

where R is the final radius of inclusions, η_m the matrix viscosity, K the viscosity ratio η_i/η_m of inclusions to the matrix, γ_{i-m} the interfacial tension between inclusions and the matrix, and ϕ_v the volume fraction of inclusions. When KR05/MS-200 blends are compression moulded, the molten material is exposed to a very slight shear flow, or most likely, stagnates. Therefore, the viscosities of the components η_{KR05} and η_{MS-200} should be much the same as their zero-shear viscosities $\eta_{0, KR05}$ and $\eta_{0, MS-200}$, respectively. $\eta_{0, KR05}$ would not differ much from the zero-shear viscosity $\eta_{0, PS}$ for the PS with the same molecular weight as KR05 has ($M_w = 1.51 \times 10^5$), since the weight fraction of a PS block component for KR05 is large ($\phi_{w, KR05} = 0.755$). This is also the case with $\eta_{0, MS-200}$. $\eta_{0, MS-200}$ and $\eta_{0, PS}$ for the PS with the same molecular weight as MS-200 has ($M_w = 2.30 \times 10^5$) should be the same order of magnitude because of the large weight fraction of a styrene component for MS-200 ($\phi_{w, MS-200} = 0.78$). Accordingly, one could assume orders of the viscosities and the viscosity ratio on compression moulding KR05/MS-200;

$$\eta_{KR05} \sim \eta_{0, \text{ PS}(M_w = 1.51 \times 10^5)} \qquad (A2)$$

$$\eta_{MS-200} \sim \eta_{0, \text{ PS}(M_w = 2.30 \times 10^5)} \qquad (A3)$$

$$K = \eta_{MS-200}/\eta_{KR05} \sim \eta_{0, \text{ PS}(M_w = 2.30 \times 10^5)}/\eta_{0, \text{ PS}(M_w = 1.51 \times 10^5)} \qquad (A4)$$

when the melt temperature is 180°C, $\eta_{0, \text{ PS}(M_w = 1.51 \times 10^5)}$ and $\eta_{0, \text{ PS}(M_w = 2.30 \times 10^5)}/\eta_{0, \text{ PS}(M_w = 1.51 \times 10^5)}$ can be estimated at about 2×10^4 Pa s and 4.2, respectively [24,25]. The viscosity

ratio is calculated by using the power law exponent of 3.4 for the molecular weight dependence of the zero-shear viscosity[26]. These data at 180°C can be reduced to those at 200°C by using the η_0-temperature relation. For the PS with the glass transition temperature of 95°C the η_0-temperature relation between 180°C and 200°C can be written as[27]

$$\log(\eta_{0,\ PS(200°C)}/\eta_{0,\ PS(180°C)}) \approx -0.675 \qquad (A5)$$

Therefore, $\eta_{0,\ PS(M_w = 1.51 \times 10^5)}$ at the mould temperature employed here (200°C) can be computed at about 4×10^3 Pa s.

Since the viscosity ratio $\eta_{0,\ PS(M_w = 2.30 \times 10^5)}/\eta_{0,\ PS(M_w = 1.51 \times 10^5)}$ at 200°C should take the same value with that at 180°C (about 4.2), K is given as

$$K = \eta_{MS-200}/\eta_{KR05} \sim 4.2(200°C) \qquad (A6)$$

Consequently, for KR05-enriched blends with the volume fraction of MS-200 $\phi_v < 0.5$, the second term of equation (A1), $[(19K + 16)(2K + 3 - 2\phi_v(K - 1))]/[10(K + 1) - 2\phi_v (5K + 2)]$ can be computed at the value of the order of 25. For KR05-enriched KR05/MS-200 blends equation (A1) can be rewritten as

$$\tau_{shape} \sim (R\eta_m/4\gamma_{i-m}) \times 25 = 6.25R\eta_{KR05}/\gamma_{MS-KR} \qquad (A7)$$

γ_{MS-KR}, the interfacial tension between MS-200 and KR05, could be equal to γ_{MS-PS} since the KR05/MS-200 interface could be formed between the PS block phase of KR05 and the MS-200 phase[1]. Equation (A7) nearly amounts to

$$\tau_{shape} \sim 6.25R\eta_{0,\ PS(M_w = 1.51 \times 10^5)}/\gamma_{MS-PS} \qquad (A8)$$

γ_{MS-PS} should be significantly smaller than $\gamma_{PMMA-PS}$ (PMMA: poly(methyl methacrylate)) since intuitively one can guess that the large fraction of styrene ($\phi_{w,\ MS-200} = 0.78$) in MS-200 could lower the interfacial tension to the PS block phase.

Interfacial tension γ_{A-B} is related to polymer–polymer interaction parameter between polymer A and B, $\chi_{blend,\ A-B}$, as[28,29]

$$\gamma_{A-B} = (\chi_{blend,\ A-B}/6)^{1/2}\rho_0 b k_B T \qquad (A9)$$

where ρ_0 is the number density of repeat units in pure polymer, b the effective length per repeat unit, k_B the Boltzmann constant, and T the absolute temperature. Since polymers of interest (PS, MS, PMMA) can be assumed to have similar ρ_0 and b, application of equation (A9) to these polymers gives

$$\gamma_{MS-PS}/\gamma_{PMMA-PS} \approx (\chi_{blend,\ MS/PS}/\chi_{blend,\ PMMA/PS})^{1/2} \qquad (A10)$$

By using a theory of phase behaviour in homopolymer/random copolymer systems[30,31],

$$\chi_{blend,\ MS/PS} = (1 - \phi_{w,\ MS})^2 \chi_{M-S} \qquad (A11)$$

where $\phi_{w,\ MS}$ is the styrene weight fraction of MS and χ_{M-S} the χ interaction parameter between MMA and styrene units, can be derived. Therefore, rearrangement of equation (A10) and introduction of equation (A11) give

$$\gamma_{MS-PS} \approx ((1 - \phi_{w,\ MS})^2 \chi_{M-S}/\chi_{M-S})^{1/2} \cdot \gamma_{PMMA-PS}$$

$$= (1 - \phi_{w,\ MS}) \cdot \gamma_{PMMA-PS} \qquad (A12)$$

For the case of MS-200, $\gamma_{MS-PS} = 0.18$ mN/m at 200°C since $\gamma_{PMMA-PS}$ at 200°C can be estimated at 0.84 mN/m[32].

By using the above-mentioned values, one can compute τ_{shape} of the 10 μm-sized MS-200 domain embedded in

KR05-enriched KR05/MS-200 blends at 200°C. From equation (A8)

$$\tau_{shape} \sim (6.25)(5 \times 10^{-6}\ m)(4 \times 10^3\ Pa\ s)/(1.8 \times 10^{-4}\ N/m)$$

$$\approx 700\ s(200°C).$$

APPENDIX B:

The diffusion distance L of the centre of mass of a polymeric molecular chain diffusing into a molten polymer varies as

$$L_{ave} \sim \langle L^2 \rangle^{1/2} \sim 2[D(T) \cdot t]^{1/2} \qquad (B1)$$

where L_{ave} is the average diffusion distance of diffusive chains, $\langle L^2 \rangle$ the mean-square displacement during the time t, D the self-diffusion (or tracer diffusion) coefficient, and T the absolute temperature[33,34]. D depends on T (i.e. $D = D(T)$) for a fixed molecular weight of the chain[35–37]. On cooling the mould, the displacement of the molten KR05 microdomain present at the specific depth from the plaque surface can be estimated by using equation (B1) with $D_{s,\ KR05}(T)$, the self-diffusion coefficient of KR05 used here. One must consider $T = T_{melt,\ d}(t)$, the melt temperature change with time at the region d mm deep from the plaque surface, in a range above the glass transition temperature (T_g) of a PS block component of KR05, where the centre of mass of a KR05 chain moves in a meaning manner.

$D_{s,\ KR05}$ can be correlated to $D_{s,\ PS(M_w = 1.51 \times 10^5)}$ and $D_{s,\ PB(M_w = 1.51 \times 10^5)}$, self-diffusion coefficients of PS and PB with the same molecular weight as KR05 has, respectively;

$$D_{s,\ PS(M_w = 1.51 \times 10^5)} < D_{s,\ KR05} < D_{s,\ PB(M_w = 1.51 \times 10^5)} \qquad (B2)$$

This can be inferred from the correlation among diffusion coefficients of styrene-isoprene (SI) block copolymer, PS and polyisoprene (PI) with the same molecular weight[38] since PB is a homologue to PI and they have much analogy in the molecular structure and T_g (ca. -80°C and ca. -70°C for PB and PI, respectively). The magnitude of $D_{s,\ KR05}$ may be more comparable with $D_{s,\ PS(M_w = 1.51 \times 10^5)}$ than with $D_{s,\ PB(M_w = 1.51 \times 10^5)}$ since KR05 has large weight fraction of a PS block component ($\phi_{w,\ KR05} = 0.755$). By using equation (B2) one can make a rough estimation of $D_{s,\ KR05}(T)$. An example at the melt temperature of 200°C (473.15°K) is shown here. $D_{s,\ PS(M_w = 1.51 \times 10^5)}$ (473.15) can be estimated at the value of the order of 3×10^{-12} cm^2/s, using the temperature dependence of D_{PS} examined with fluorescein labelled PS[39] or deuterated PS[36] as a tracer. $D_{s,\ PB(M_w = 1.51 \times 10^5)}$ (473.15) may be of the order of 10^{-10} cm^2/s, which was gauged with the $D_{s,\ PI}$ data in the literature[38] on the assumption that $D_{s,\ PB}$ is similar to $D_{s,\ PI}$ for the materials with the same molecular weight and that D_S roughly follows -2 power proportionality (i.e. $D_s \propto$ (molecular weight)$^{-2}$)[39]. Therefore, from equation (B2), $3 \times 10^{-12} < D_{s,KR05}$ (473.15) $< 10^{-10}$ cm^2/s is given.

Under the moulding condition that the mould temperature dropped down from 200°C to 50°C in 3 min as employed in this study, assuming that the coolant running through the cooling circuit was kept at 25°C on cooling, the average temperature of the steel mould $T_{mould}(t)$ is written as

$$T_{mould}(t) = 175e^{-0.0108t} + 298.15 \qquad (B3)$$

If the temperature of the melt surface which was touched to the cavity wall, $T_{melt,\ 0\ mm}(t)$, was the same as the

Table 1 The melt temperature, the self-diffusion coefficient and the approximate increment of the diffusion distance at regions inside the molten 4.0 mm thick plaque of PS, which were calculated each time 2 s elapsed for the first 30 s on cooling the mould

t (s)	$T_{melt, 0\,mm}(t)^a$ (K)	$T_{melt,\,d}(t)^b$ (K)			$D_{s,\,PS(M_w=1.51\times10^5)}(T)^c$ ($\times 10^{-14}$ cm^2/s)			$2.828\,[D_{s,\,PS(M_w=1.51\times10^5)}(T)]^{1/2\,d}$ (μm)		
		$d = 0.5$	$d = 1.0$	$d = 2.0$	$d = 0.5$	$d = 1.0$	$d = 2.0$	$d = 0.5$	$d = 1.0$	$d = 2.0$
2	469.4	472.0	472.8	473.15	310	320	330	0.050	0.051	0.051
4	465.7	469.4	471.6	473.1	260	310	330	0.046	0.050	0.051
6	462.2	466.7	470.0	472.3	210	260	310	0.041	0.046	0.050
8	458.7	463.9	467.7	471.3	140	190	280	0.033	0.039	0.047
10	455.2	460.8	465.3	469.2	100	160	230	0.028	0.036	0.043
12	451.9	457.9	462.5	467.0	82	140	190	0.026	0.034	0.039
14	448.6	455.0	459.9	465.0	68	100	160	0.023	0.028	0.036
16	445.4	451.8	456.8	461.8	45	82	140	0.019	0.026	0.034
18	442.2	448.7	454.0	458.9	36	54	92	0.017	0.021	0.027
20	439.1	445.6	450.7	455.4	25	41	68	0.014	0.018	0.023
22	436.1	442.4	447.6	452.0	16	31	45	0.011	0.016	0.019
24	433.2	439.6	444.8	449.2	13	22	36	0.010	0.013	0.017
26	430.3	436.7	441.4	446.2	9.6	15	27	0.0088	0.011	0.015
28	427.4	433.3	438.4	442.5	6.5	9.6	18	0.0072	0.0088	0.012
30	424.7	430.5	434.9	439.2	4.3	6.5	13	0.0059	0.0072	0.010
Total (μm)								0.34	0.40	0.48

^{a} Temperature of the molten plaque surface (depth $d = 0$ mm).
^{b} Temperature at regions d mm deep from the plaque surface.
^{c} Self-diffusion coefficient of PS ($M_w = 1.51 \times 10^5$).
^{d} Approximate increment of the diffusion distance of PS ($M_w = 1.51 \times 10^5$) for 2 s.

temperature of the cavity wall,

$$T_{melt,\,0\,mm}(t) = 175e^{-0.0108t} + 298.15 \qquad (B4)$$

Every 2 s for the first 30 s on cooling the mould $T_{melt,\,0\,mm}(t)$ is calculated by equation (B4) and shown in *Table 1*. The temperature of the melt at the regions of d mm in depth from the surface of the 4.0 mm thick plaque, $T_{melt,\,d}(t)$, and the corresponding $D_s(T_{melt,\,d}(t))$ are approximated numerically in the following. Since it is most likely that thermal diffusivity of styrenic KR05/MS-200 blends is much the same as that of conventional styrenic polymers ($\sim 8 \times 10^{-4}$ cm^2/s over T_g of PS)[40], $T_{melt,\,d}(t)$ for $d = 0.5$, 1.0[41] and 2.0 mm[42,43] can be calculated as shown in *Table 1*. For short duration t introduction of equation (B2) to equation (B1) gives

$$L_{ave,\,KR05} \sim 2[D_{s,\,KR05}(T_{melt,\,d}(t))\cdot t]^{1/2}$$
$$> 2[D_{s,\,PS(M_w=1.51\times10^5)}(T_{melt,\,d}(t))\cdot t]^{1/2} \qquad (B5)$$

where $L_{ave,\,KR05}$ is the average diffusion distance of KR05 molecules on cooling the mould. For the first 2 s ($0 \le t \le 2$) on cooling the mould the relationship between the first and the second terms of equation (B5) can be rewritten as

$$L_{ave,\,KR05}\,(0 \le t \le 2) > 2[D_{s,\,KR05}(T_{melt,\,d}(2))\cdot 2]^{1/2} \quad (B6)$$

where $L_{ave,\,KR05}$ ($0 \le t \le 2$) is the actual diffusion distance of the KR05 molecule for the first 2 s ($0 \le t \le 2$) on cooling the mould. An unequal sign should be put in equation (B6) since $D_{s,\,KR05}(T_{melt,\,d}(t))$ decreases with the time t passing away and therefore $D_{s,\,KR05}(T_{melt,\,d}(2))$ is the smallest value of $D_{s,\,KR05}(T_{melt,\,d}(t))$ for ($0 \le t \le 2$). From equations (B5) and (B6)

$$L_{ave,\,KR05}(0 \le t \le 2) > 2[D_{s,\,PS(M_w=1.51\times10^5)}(T_{melt,\,d}(2))\cdot 2]^{1/2}$$
$$= 2.828[D_{s,\,PS(M_w=1.51\times10^5)}(T_{melt,\,d}(2))]^{1/2} \qquad (B7)$$

equation (B5) is applied similarly every 2 s for the first 30 s

on cooling, leading to

$$L_{ave,\,KR05}((2k-2) \le t \le 2k)$$
$$> 2.828[D_{s,\,PS(M_w=1.51\times10^5)}(T_{melt,\,d}(2k))]^{1/2} \qquad (B8)$$

for $k = 1, 2, 3, ..., 15$

Therefore,

$$L_{ave,\,KR05} > L_{ave,\,KR05}(0 \le t \le 30) > 2.828$$
$$\times \sum_{k=1}^{15} [D_{s,\,PS(M_w=1.51\times10^5)}(T_{melt,\,d}(2k))]^{1/2} \qquad (B9)$$

It should be noted that the chain dynamic modes responsible for D and the zero-shear viscosity η_0 would be the same since D/T and η_0^{-1} seem to obey the same temperature dependence in a range not far above T_g of the PS ($T \le T_g + 100$ K), being described by the Williams–Landel–Ferry (WLF) equation[35–37]. $D_{s,\,PS(M_w=1.51\times10^5)}(T)$ was obtained here from the curve of D/T as a function of T in the literature[36] which exhibits good fit of the WLF equation. The estimated value of $D_{s,\,PS(M_w=1.51\times10^5)}(T_{melt,\,d}(2k))$ and the approximate increment of the diffusion distance each time 2 s elapsed, $2.828\,[D_{s,\,PS(M_w=1.51\times10^5)} \times (T_{melt,\,d}(2k))]^{1/2}$, are shown in *Table 1* for $k = 1, 2, 3, ..., 15$. From the summation $2.828 \times \sum_{k=1}^{15}[D_{s,\,PS(M_w=1.51\times10^5)}(T_{melt,\,d}(2k))]^{1/2}$ and equation (B9), $L_{ave,\,KR05}$ s for $d = 0.5$, 1.0 and 2.0 mm should be over 0.34, 0.40 and 0.48 μm, respectively.

REFERENCES

1. Yamaoka, I., *Polymer*, 1995, **36**, 3359.
2. Yamaoka, I., *Polymer*, 1996, **37**, 5343.
3. Kuleznev, V.N. and Vlasov, S.V., *Makromol. Chem. Macromol. Symp.*, 1989, **28**, 85.
4. Lee, M.-P., Hiltner, A., Baer, E. and Kao, C.-I., *J. Mater. Sci.*, 1993, **28**, 1491.

5. Hsu, W.Y. and Wu, S., *Polym. Eng. Sci.*, 1993, **33**, 293.
6. Yamaoka, I. and Kimura, M., *Polymer*, 1993, **34**, 4399.
7. Byun, H.S., Burford, R.P. and Mai, Y.-W., *Mater. Forum*, 1989, **13**, 26.
8. Chui, S.T., Hsu, W.Y. and Tian, D., *J. Appl. Phys.*, 1995, **78**(7), 4715.
9. Takayanagi, M. and Goto, K., *Polym. Sci. Technol. Mol. Charact. Compos. Interfaces*, 1985, **27**, 247.
10. Lin, Q. and Yee, A.F., *Polym. Compos.*, 1994, **15**(2), 156.
11. Shen, M. and Kawai, H., *AIChE J.*, 1978, **24**, 1.
12. Aggarwal, S.L., *Polymer*, 1976, **17**, 938.
13. Godovsky, Y.K., *Makromol. Chem. Suppl.*, 1984, **6**, 117.
14. Allan, P., Arridge, R.G.C., Ehtaiatkar, F. and Folkes, M.J., *J. Phys. D: Appl. Phys.*, 1991, **24**, 1381.
15. Honeker, C., Villar, M.A. and Thomas, E.L., *Polym. Prepr. Am. Chem. Soc. Div. Polym. Chem.*, 1993, **34**(1), 786.
16. Hashimoto, T., Shibayama, M. and Kawai, H., *Macromolecules*, 1980, **13**, 1237.
17. Hashimoto, T., Nagatoshi, K., Todo, A., Hasegawa, H. and Kawai, H., *Macromolecules*, 1974, **7**, 364.
18. Inoue, T., Soen, T., Hashimoto, T. and Kawai, H., *J. Polym. Sci.*, 1969, **7**, 1283.
19. Keller, A., Pedemonte, E. and Willmouth, F.M., *Kolloid Z.*, 1970, **238**, 385.
20. Delaby, I., Ernst, B., Germain, Y. and Muller, R., *J. Rheol.*, 1994, **38**(6), 1705.
21. Delaby, I., Froelich, D. and Muller, R., *Macromol. Symp.*, 1995, **100**, 131.
22. Graebling, D., Muller, R. and Palierne, J.F., *Macromolecules*, 1993, **26**, 320.
23. Riemann, R.-E., Cantow, H.-J. and Friedrich, C., *Polym. Bull.*, 1996, **36**, 637.
24. Allen, V.R. and Fox, T.G., *J. Chem. Phys.*, 1964, **41**(2), 337.
25. Jackson, J.K., De Rosa, M.E. and Winter, H.H., *Macromolecules*, 1994, **27**, 2426.
26. Odani, H., Nemoto, N. and Kurata, M., *Bull. Inst. Chem. Res. Kyoto Univ.*, 1972, **50**(2), 117.
27. Magill, J.H. and Li, H.-M., *J. Polym. Sci. Part B: Polym.Lett.*, 1973, **11**, 667.
28. Helfand, E. and Tagami, Y., *J. Polym. Sci. Part B: Polym. Lett.*, 1971, **9**, 741.
29. Sammler, R.L., Dion, R.P., Carriere, C.J. and Cohen, A., *Rheol. Acta*, 1992, **31**(6), 554.
30. Kambour, R.P., Bendler, J.T. and Bopp, R.C., *Macromolecules*, 1983, **16**, 753.
31. ten Brinke, G., Karasz, F.E. and MacKnight, W.J., *Macromolecules*, 1983, **16**, 1827.
32. Wu, S., *J. Macromol. Sci. Rev. Macromol. Chem.*, 1974, **C 10**(1), 1.
33. Karim, A., Mansour, A. and Felcher, G.P., *Phys. Rev. B*, 1990, **42**(10), 6846.
34. Hong, P.P., Boerio, F.J. and Clarson, S.J., *Polym. Prepr. Am. Chem. Soc. Div. Polym. Chem.*, 1991, **32**(3), 314.
35. Nemoto, N., Landry, M.R., Noh, I. and Yu, H., *Polym. Commun.*, 1984, **25**, 141.
36. Green, P.F. and Kramer, E.J., *J. Mater. Res.*, 1986, **1**(1), 202.
37. Green, P.F., Russell, T.P., Jérôme, R. and Granville, M., *Macromolecules*, 1989, **22**, 908.
38. Ehlich, D., Takenaka, M. and Hashimoto, T., *Macromolecules*, 1993, **26**, 492.
39. Antonietti, M., Coutandin, J. and Sillescu, H., *Makromol. Chem. Rapid Commun.*, 1984, **5**, 525.
40. Ito, K., *Purasuchikkusu*, 1968, **19**(7), 65.
41. Ito, K., *Purasuchikkusu*, 1967, **18**(1), 63.
42. Ito, K., *Purasuchikkusu*, 1967, **18**(3), 63.
43. Ito, K., *Purasuchikkusu*, 1967, **18**(11), 57.